ЖУРНАЛ СТРУКТУРНОЙ ХИМИИ

2015. Том 56, № 7 *Декабрь* *С. 1339 – 1353*

UDC 541.6:548.737

STRUCTURAL AND ELECTRONIC PROPERTIES OF HEPTACHLOR

Y. Gülseven Sıdır[1], İ. Sıdır[1], F. Demiray[2]

[1]*Bitlis Eren University, Faculty of Arts and Sciences, Department of Physics, Bitlis, Turkey*
E-mail: ygsidir@bitliseren.edu.tr, yadigar.gulseven@gmail.com
[2]*Abant İzzet Baysal University, Vocational Higher School, Mudurnu, Bolu, Turkey*

Received April, 24, 2014 *Revised May, 26, 2014*

In this work, the molecular geometry of heptachlor is investigated using *ab initio* HF, DFT, LDA, and GGA methods. The natural bond orbital (NBO) analysis is performed at the B3LYP/6-311++G(*d*,*p*) level of theory. The first order hyperpolarizability β_{total}, the mean polarizability $\langle\alpha\rangle$, the anisotropy of the polarizability $\Delta\alpha$, and the dipole moment μ, are calculated by B3LYP/6-311++G(*d*,*p*) and HF/6-311++G(*d*,*p*) methods. The first order hyperpolarizability (β_{total}) is calculated based on the finite field approach. UV spectral parameters along with HOMO, LUMO energies for heptachlor are determined in vacuum and the solvent phase using HF, DFT, and TD-DFT/B3LYP methods implemented with the 6-311++G(*d*,*p*) basis set. Atomic charges and electron density of heptachlor in vacuum and ethanol are calculated using DFT/B3LYP and TD-DFT/B3LYP methods and the 6-311++G(*d*,*p*) basis set. In addition, after the frontier molecular orbitals (FMOs), the molecular electrostatic potential (MEP), the electrostatic potential (ESP), the electron density (ED), and the solvent accessible surface of heptachlor are visualized as a results of the B3LYP/6-311++G(*d*,*p*) calculation. Densities of states (DOS), the external electric field (EF) effect on the HOMO-LUMO gap, and the dipole moment are investigated by LDA and GGA methods.

DOI: 10.15372/JSC20150707

K e y w o r d s: heptachlor, density of states, hyperpolarizability, NBO analysis, DFT, ESP.

INTRODUCTION

Heptachlor (1,4,5,6,7,8,8-heptachloro-3a,4,7,7a-tetrahydro-1H-4,7-methanoindene), which is not found naturally in the earth, is a chlorinated dicyclopentadiene insecticide. Heptachlor and its congeners (such as heptachlor epoxide, chlordane, toxaphene, etc.) were used for about 30 years as a contact insecticide, mainly in the control of soil insects and termites. These pesticides were used in the termite control and in the control of ants both commercially and domestically [1, 2] as well as for the pest control on cotton crops [3].

Although the use of pesticides has been prohibited and severely restricted in many countries since the 1980′s, they are still detected as a contaminant in some food commodities. This is due to their persistence. Heptachlor is one of several organochlorine pesticides that are persistent in the environment. This compound is also a bioconcentrate in the environment and accumulates in the food-chain [4]. The chlorinated hydrocarbon structure of the pesticides has enabled them to persist in the environment, contaminating all forms of life [5] such as marine mammals [6, 7], humans [8], cattle [9], and birds [10]. The structure of the chlorinated hydrocarbons enables them to resist environmental degradation and create a long-lasting problem, especially with respect to the toxicities associated with

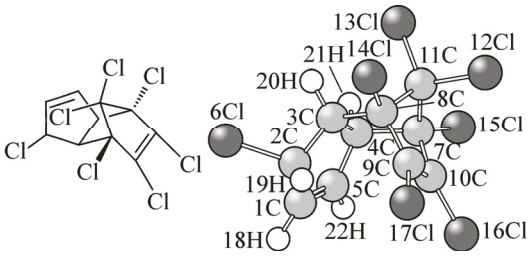

Fig. 1. The B3LYP/6-311++G(*d,p*) optimized structure with atoms numbering of 1,4,5,6,7,8,8-heptachloro-3a,4,7,7a-tetrahydro-1H-4,7-methanoindene (heptachlor)

these compounds [5]. The studies on rats and mice indicate that heptachlor and its congeners are liver toxicants and potential human carcinogens [11—14]. It is said previously that these compounds are tumor promoters [15—17].

Heptachlor released into the environment can be transformed into hydroxyl radicals by a photochemical process and it is transformed in the presence of water to heptachlor epoxide that is more stable than heptachlor and only slightly water-soluble. Both compounds are persistent and concentrate in the environment [4]. However, the persistence of heptachlor can be attributed to the presence of chlorine atoms, non-planar geometry, and chiral centers. These properties make this compound attractive to study on. Thus, we aimed at investigating the structural and electronic properties of heptachlor.

EXPERIMENTAL

1,4,5,6,7,8,8-Heptachloro-3a,4,7,7a-tetrahydro-1H-4,7-methanoindene (heptachlor) (Fig. 1) was purchased from Sigma-Aldrich with the 99 % purity and used without further purification. UV-vis. absorption spectra were recorded on a Perkin Elmer Lambda 35 UV-vis. spectrophotometer. The concentration in the ethanol solution was prepared as 10^{-5} M.

CALCULATION METHOD

Our calculations are based on the spin polarized density functional theory (DFT) in the local density approximation (LDA) and the generalized gradient approximation (GGA) as implemented in the SIESTA code [18]. We used the Perdew-Zunger [19] parametrization for the functional and the revised [20] Perdew-Burke-Ernzerhof [21] GGA functional. Electronic wave functions were expanded to a double-ζ basis set augmented by polarization orbitals. The interaction between the core and valance electrons was handled by Troullier-Martins norm-conserving pseudopotentials [22] in their fully separable form [23]. The geometry optimizations in the conjugate-gradient algorithm were continued until all force components became less than 0.01 eV/Å.

All of the HF, DFT, TD-DFT calculations were performed using the Gaussian 09W program package [24].

RESULTS AND DISCUSSION

Optimized geometry. The schematic depiction of optimized heptachlor is shown in Fig. 1. The structural parameters obtained by the X-ray single crystal diffraction method [25] and optimized geometrical parameters without symmetry constraints are given in Table 1. A comparison of the experimental and optimized geometrical parameters indicates that the optimized bond lengths and bond angles are in good agreement with the experimental results. As seen from Table 1, the consideration of the geometrical parameters related to H atoms lowers the correlation coefficient because the optimized C—H bond lengths and C—C—H bond angles are not consistent with the experimental results. B3LYP/6-311++G(*d,p*) calculated geometrical parameters are found to be most consistent with the experimental ones for bond angles and dihedral angles when C—C—H related parameters are not considered in the correlation. However, the HF/6-311++G(*d,p*) level of theory is relatively successful in calculating bond lengths. The differences between the experimental and theoretically obtained C—H bond lengths and C—C—H bond angles can be attributed to conjugation on the C(1)—C(2)—C(3)—C(4)—C(5) ring as a result of the non-planar geometry and electronegativity of chlorine atoms. It is also important to note that experimental data are recorded in the solid state of the molecule while the theoretical calculation is performed in the vacuum phase.

Table 1

Bond distances (Å) *and bond angles* (deg.) *of heptachlor*

r (Å)	X-ray [a]	B3LYP/6-311++G(*d*,*p*)	HF/6-311++G(*d*,*p*)	LDA	GGA
C(1)—C(2)	1.484	1.498	1.501	1.494	1.509
C(2)—C(3)	1.573	1.543	1.541	1.531	1.551
C(3)—C(4)	1.574	1.567	1.557	1.554	1.571
C(4)—C(5)	1.501	1.501	1.502	1.493	1.509
C(1)=C(5)	1.322	1.333	1.317	1.350	1.359
C(2)—Cl(6)	1.815	1.843	1.811	1.800	1.824
C(2)—H(19)	0.960	1.088	1.077	1.122	1.115
C(1)—H(18)	0.820	1.082	1.073	1.110	1.106
C(5)—H(22)	0.795	1.083	1.074	1.111	1.107
C(4)—H(21)	1.142	1.090	1.080	1.121	1.116
C(3)—H(20)	0.977	1.086	1.076	1.118	1.112
C(3)—C(8)	1.533	1.562	1.555	1.546	1.566
C(8)—C(11)	1.561	1.571	1.556	1.546	1.570
C(11)—C(7)	1.562	1.567	1.554	1.544	1.568
C(7)—C(4)	1.560	1.574	1.560	1.560	1.580
C(8)—Cl(14)	1.749	1.775	1.759	1.748	1.771
C(11)—Cl(12)	1.774	1.789	1.771	1.755	1.779
C(11)—Cl(13)	1.776	1.795	1.775	1.767	1.790
C(7)—Cl(15)	1.764	1.775	1.759	1.746	1.769
C(8)—C(9)	1.521	1.529	1.528	1.513	1.532
C(9)=C(10)	1.327	1.336	1.314	1.355	1.366
C(10)—C(7)	1.522	1.525	1.524	1.509	1.529
C(9)—Cl(17)	1.710	1.714	1.707	1.696	1.714
C(10)—Cl(16)	1.700	1.711	1.704	1.691	1.709
CC with C—H bonds		0.9528	0.9544	0.9535	0.9557
CC except for C—H bonds		0.9927	0.9934	0.9897	0.9914
θ (deg.)	X-ray [a]	B3LYP/6-311++G(*d*,*p*)	HF/6-311++G(*d*,*p*)	LDA	GGA
1	2	3	4	5	6
C(1)—C(2)—C(3)	103.58	104.72	104.37	104.57	104.55
C(2)—C(3)—C(4)	105.77	105.99	106.11	106.69	106.58
C(3)—C(4)—C(5)	103.74	104.11	104.12	104.29	104.27
C(4)—C(5)=C(1)	112.61	112.42	112.45	111.86	112.05
C(5)=C(1)—C(2)	114.28	112.74	112.93	112.34	112.48
C(1)—C(2)—Cl(6)	110.22	110.12	110.57	109.41	110.08
C(3)—C(2)—Cl(6)	110.83	111.38	111.67	111.33	111.58
C(1)—C(2)—H(19)	110.67	113.74	112.85	113.88	113.48
Cl(6)—C(2)—H(19)	110.67	103.13	103.86	105.25	104.37
C(2)—C(3)—H(20)	110.17	110.97	110.62	111.41	110.85
C(3)—C(2)—H(19)	110.67	113.92	113.71	112.48	112.92
C(3)—C(4)—H(21)	106.95	112.76	112.60	113.70	113.26
C(4)—C(3)—H(20)	116.19	111.75	111.77	112.83	112.33
C(4)—C(5)—H(22)	119.02	122.51	122.56	122.69	122.66
C(5)—C(4)—H(21)	114.35	112.43	111.69	114.42	113.22
C(5)—C(1)—H(18)	112.23	125.74	125.69	125.83	125.80
C(1)—C(5)—H(22)	126.91	125.07	124.98	125.37	125.27
C(2)—C(1)—H(18)	132.62	121.51	121.37	121.76	121.68
C(8)—C(3)—H(20)	114.55	108.67	108.85	108.68	108.68
C(7)—C(4)—H(21)	113.09	107.92	108.43	107.15	107.39

Continued Table 1

1	2	3	4	5	6
C(3)—C(4)—C(7)	102.20	102.76	102.75	102.75	102.83
C(4)—C(7)—C(11)	100.81	101.03	101.19	100.96	100.83
C(7)—C(11)—C(8)	92.86	92.27	92.32	92.91	92.58
C(11)—C(8)—C(3)	100.62	101.01	101.14	100.96	101.04
C(8)—C(3)—C(4)	103.35	102.83	102.67	102.73	102.80
C(8)—C(3)—C(2)	114.93	116.25	116.56	114.24	115.38
C(7)—C(4)—C(5)	114.89	116.40	116.93	114.05	115.51
C(4)—C(7)—C(10)	108.01	107.69	107.59	106.74	107.54
C(3)—C(8)—C(9)	107.84	108.32	108.13	107.40	108.10
C(7)—C(10)=C(9)	107.38	107.56	107.69	106.84	106.99
C(10)=C(9)—C(8)	108.42	107.69	107.75	107.21	107.33
C(9)—C(8)—C(11)	98.52	98.98	98.93	99.95	99.47
C(11)—C(7)—C(10)	99.27	99.26	99.20	100.19	99.76
C(3)—C(8)—Cl(14)	115.13	114.32	114.25	115.13	114.72
C(9)—C(8)—Cl(14)	115.86	115.86	115.94	115.11	115.31
C(11)—C(8)—Cl(14)	116.64	116.32	116.46	116.32	116.25
C(8)—C(11)—Cl(13)	113.46	114.01	114.16	113.05	113.47
C(7)—C(11)—Cl(13)	113.79	113.89	114.06	112.76	113.27
C(8)—C(11)—Cl(12)	114.27	114.22	114.30	114.01	114.15
C(7)—C(11)—Cl(12)	114.66	114.37	114.43	114.04	114.28
C(4)—C(7)—Cl(15)	114.43	114.26	114.23	115.00	114.70
C(10)—C(7)—Cl(15)	115.68	116.08	116.11	115.63	115.67
C(11)—C(7)—Cl(15)	116.64	116.45	116.52	116.29	116.32
C(7)—C(10)—Cl(16)	123.74	124.42	124.36	123.03	123.82
C(9)=C(10)—Cl(16)	128.42	127.88	127.83	129.10	128.68
C(8)—C(9)—Cl(17)	124.34	124.53	124.60	123.18	123.77
C(10)=C(9)—Cl(17)	126.97	127.69	127.71	128.89	128.49
CC[b] with C—C—H angles		0.7966	0.8371	0.8359	0.8377
CC[b] except for C—C—H angles		0.9944	0.9935	0.9896	0.9937

[a] [25].
[b] Correlation coefficient.

In the heptachlor molecule studied here, chlorine atoms along with a resonance effect on C—C bonds due to the non-planar geometry cause changes in the C—H bonds. The equilibrium structure for the ground state shows that only C(1)—H(18) and C(5)—H(22) bonds are in the C(1)—C(2)—C(3)—C(4)=C(5) ring plane, whereas the others lie out of the plane. It is observed that the C(5)—H(22) bond is the shortest one (0.795 Å), and the C(4)—H(21) bond is the longest one (1.142 Å) among the C—H bonds in heptachlor. These differences can be attributed to the effects of the non-planar geometry and electronegativity of chlorine atoms. The optimized C—H bond lengths are found to be longer than the experimental ones.

As a result of the X-ray data and calculations, C(1)—C(5) and C(9)—C(10) bonds show typical double bond characteristics with lengths of 1.322 Å and 1.327 Å. C(1)—C(2) and C(4)—C(5) bonds are relatively shorter than the other C—C single bonds since these bonds are affected by electronegativity of the Cl(6) atom and the resonance effect of the π bond.

The H atom substitution for the Cl atom gives rise to a considerable increase in the C—Cl bond length. This has been observed especially in the non-planar geometry along with benzene derivatives due to the intramolecular interactions [26].

The C(3)—C(4)—C(7)—C(11)—C(8) ring with the bond angles (C(3)—C(4)—C(7), C(4)—C(7)—C(11), C(7)—C(11)—C(8), C(11)—C(8)—C(3), and C(8)—C(3)—C(4)) changing in the range of 92.9—103.4° is close to the tetrahedral geometry and resembles the *chair* conformation. A similar

geometry can be seen for the C(7)—C(10)=C(9)—C(8)—C(11) ring with the bond angles changing in the range of 92.9—108.4°.

Natural bond orbital (NBO) analysis. The NBO analysis has been performed on the molecule using the NBO 3.1 program. The important results have been listed in Table 2.

Table 2

Second order perturbation theory analysis of the Fock matrix in the selected NBO *basis calculated at the* B3LYP/6-311++G(*d*,*p*) *level of theory for heptachlor*

Donor (*i*)	Type	ED/e	Acceptor (*j*)	Type	ED/e	$E^{(2)}$, kJ · mol^{-1} [a]	$E(j) - E(i)$, a.u. [b]	$F(i,j)$, a.u. [c]
1	2	3	4	5	6	7	8	9
C(1)—C(5)	σ	0.99090	C1—C2	σ*	0.01206	0.73	1.14	0.036
			C2—H18	σ*	0.00739	0.80	1.17	0.039
			C2—Cl6	σ*	0.02785	0.54	0.88	0.028
			C2—H19	σ*	0.01439	0.34	1.10	0.025
			C4—C5	σ*	0.01033	0.91	1.16	0.041
			C4—C7	σ*	0.03025	0.62	1.05	0.032
			C4—H21	σ*	0.01185	0.26	1.12	0.022
			C5—H22	σ*	0.00739	0.79	1.17	0.039
	π	0.96288	C2—Cl6	σ*	0.02785	2.93	0.42	0.045
			C2—H19	σ*	0.01439	1.63	0.64	0.041
			C4—C7	σ*	0.03025	2.06	0.59	0.044
			C4—H21	σ*	0.01185	1.81	0.66	0.044
			C9—C10	σ*	0.02204	0.32	0.27	0.012
C(2)—Cl(6)	σ	0.99107	C1—C5	σ*	0.00583	0.34	1.33	0.027
			C1—C5	π*	0.02411	0.96	0.73	0.034
			C3—C4	σ*	0.01204	0.39	1.01	0.025
C(7)—Cl(15)	σ	0.97900	C3—C4	σ*	0.01204	0.45	1.11	0.028
			C8—C11	σ*	0.04203	0.40	1.01	0.026
			C9—C10	σ*	0.02204	0.49	1.33	0.033
C(8)—Cl(14)	σ	0.99400	C3—C4	σ*	0.01204	0.46	1.10	0.029
			C7—C11	σ*	0.04130	0.40	1.01	0.026
			C9—C10	σ*	0.02204	0.50	1.33	0.033
C(9)—C(10)	σ	0.98680	C7—C10	σ*	0.03238	1.17	1.09	0.046
			C7—Cl15	σ*	0.02286	1.34	0.92	0.044
			C8—C9	σ*	0.03284	1.17	1.09	0.046
			C8—Cl14	σ*	0.02310	1.33	0.92	0.044
			C9—Cl17	σ*	0.01672	0.40	0.95	0.025
			C10—Cl16	σ*	0.01661	0.40	0.96	0.025
			C11—Cl13	σ*	0.03762	0.37	0.88	0.023
	π	0.96877	C3—C8	σ*	0.02451	1.20	0.64	0.035
			C3—H20	σ*	0.00858	0.31	0.71	0.019
			C4—C7	σ*	0.03025	1.19	0.64	0.035
			C4—H21	σ*	0.01185	0.30	0.71	0.018
			C7—C11	σ*	0.04130	0.27	0.55	0.016
			C7—Cl15	σ*	0.02286	0.57	0.47	0.021
			C8—C11	σ*	0.04203	0.30	0.55	0.016
			C8—Cl14	σ*	0.02310	0.58	0.48	0.021
			C11—Cl13	σ*	0.03762	0.82	0.44	0.024
C(9)—Cl(17)	σ	0.99544	C7—C10	σ*	0.03238	0.84	1.15	0.040
			C9—C10	σ*	0.02204	0.94	1.37	0.046

Continued Table 2

1	2	3	4	5	6	7	8	9
C(10)—Cl(16)	σ	0.99543	C8—C9	σ*	0.03284	0.86	1.15	0.040
			C9—C10	σ*	0.02204	0.96	1.37	0.046
C(11)—Cl(12)	σ	0.99324	C3—C8	σ*	0.02451	0.65	1.09	0.034
			C4—C7	σ*	0.03025	0.63	1.09	0.033
C(11)—Cl(13)	σ	0.99316	C7—C10	σ*	0.03238	0.55	1.10	0.031
			C8—C9	σ*	0.03284	0.55	1.10	0.032
Cl(6)	LP(2)	0.98539	C2—C3	σ*	0.01453	1.13	0.66	0.034
			C2—H19	σ*	0.01439	2.30	0.67	0.050
Cl(6)	LP(3)	0.98203	C1—C2	σ*	0.01206	2.08	0.71	0.049
			C1—C5	π*	0.02411	0.69	0.35	0.020
			C2—C3	σ*	0.01453	1.04	0.66	0.033
Cl(12)	LP(1)	0.99413	C7—C11	σ*	0.04130	0.51	1.20	0.032
			C8—C11	σ*	0.04203	0.53	1.20	0.032
			C11—Cl13	σ*	0.03762	0.52	1.09	0.030
Cl(12)	LP(2)	0.97262	C4—C7	σ*	0.03025	0.39	0.64	0.020
			C7—C11	σ*	0.04130	2.05	0.55	0.052
			C11—Cl13	σ*	0.03762	2.78	0.44	0.044
Cl(12)	LP(3)	0.97251	C3—C8	σ*	0.02451	0.41	0.64	0.020
			C7—C11	σ*	0.04130	0.33	0.55	0.017
			C8—C11	σ*	0.04203	3.22	0.54	0.053
			C11—Cl13	π*	0.03762	2.29	0.44	0.040
Cl(13)	LP(1)	0.99382	C7—C11	σ*	0.04130	0.54	1.20	0.033
			C8—C11	σ*	0.04203	0.56	1.20	0.033
			C11—Cl12	σ*	0.03321	0.45	1.10	0.028
Cl(13)	LP(2)	0.97044	C7—C10	σ*	0.03238	0.25	0.65	0.016
			C7—C11	σ*	0.04130	2.69	0.55	0.049
			C8—C11	σ*	0.04203	2.59	0.55	0.048
Cl(14)	LP(1)	0.99472	C3—C8	σ*	0.02451	0.61	1.27	0.036
			C8—C9	σ*	0.03284	0.43	1.28	0.030
			C8—C11	σ*	0.04203	0.46	1.18	0.030
Cl(14)	LP(2)	0.97687	C3—C4	σ*	0.01204	0.37	0.64	0.019
			C3—C8	σ*	0.02451	2.96	0.63	0.055
			C8—C9	σ*	0.03284	2.36	0.64	0.050
Cl(14)	LP(3)	0.96983	C3—C8	σ*	0.02451	0.35	0.64	0.019
			C7—C11	σ*	0.04130	0.42	0.55	0.019
			C8—C9	σ*	0.03284	1.70	0.65	0.042
			C8—C11	σ*	0.04203	3.97	0.54	0.059
Cl(15)	LP(1)	0.99484	C4—C7	σ*	0.03025	0.56	1.27	0.034
			C7—C10	σ*	0.03238	0.41	1.28	0.029
			C7—C11	σ*	0.04130	0.45	1.18	0.030
Cl(15)	LP(2)	0.97709	C3—C4	σ*	0.01204	0.35	0.64	0.019
			C4—C7	σ*	0.03025	3.02	0.64	0.056
			C7—C10	σ*	0.03238	2.23	0.65	0.048
Cl(15)	LP(3)	0.97074	C4—C7	σ*	0.03025	0.31	0.64	0.018
			C7—C10	σ*	0.03238	1.78	0.65	0.043
			C7—C11	σ*	0.04130	3.86	0.55	0.059
			C8—C11	σ*	0.04203	0.42	0.55	0.019
Cl(16)	LP(1)	0.99461	C7—C10	σ*	0.03238	1.07	1.27	0.047

Continued Table 2

1	2	3	4	5	6	7	8	9
			C9—C10	σ*	0.02204	1.58	1.49	0.062
Cl(16)	LP(2)	0.97316	C7—C10	σ*	0.03238	4.09	0.66	0.066
			C9—C10	σ*	0.02204	3.13	0.88	0.066
Cl(16)	LP(3)	0.93978	C9—C10	π*	0.11279	11.81	0.32	0.080
Cl(17)	LP(1)	0.99445	C8—C9	σ*	0.03284	1.10	1.27	0.048
			C9—C10	σ*	0.02204	1.51	1.49	0.061
Cl(17)	LP(2)	0.97313	C8—C9	σ*	0.03284	4.08	0.66	0.066
			C9—C10	σ*	0.02204	3.16	0.88	0.067
Cl(17)	LP(3)	0.94108	C9—C10	π*	0.11279	11.53	0.32	0.079

[a] $E^{(2)}$ means energy of hyperconjugative interactions (stabilization energy).
[b] Energy difference between donor (*i*) and acceptor (*j*) NBO orbitals.
[c] $F(i,j)$ is the Fock matrix element between *i* and *j* orbitals.

Heptachlor has two π bonds located on C(1)—C(5) and C(9)—C(10) bonds. These bonds contribute to the delocalization in the molecule with ~0.97 e^- ED. The σ electron delocalization is maximum around C(2)—Cl(6), C(4)—C(7), C(2)—H(19), C(1)—C(2), C(7)—C(11), C(11)—Cl(13), C(8)—C(11), C(3)—C(8), C(8)—C(9), C(7)—C(10), and C(9)—C(10) of heptachlor, which is revealed by ED at the conjugated σ bonds (2—5 kJ/mol). The most important interaction energy, related to resonance in the molecule, is electron donating from LP(3) Cl(16) and LP(3) Cl(17) to the antibonding acceptor π*(C(9)—C(10)), resulting in a stabilization energy of 11.81 kJ/mol and 11.53 kJ/mol respectively, which denotes a larger delocalization.

Hyperpolarizability calculations. The first order hyperpolarizability (β_{total}) of heptachlor along with the related properties (μ, ⟨α⟩ and Δα) are calculated based on the finite field approach. The first order hyperpolarizability is a third rank tensor that can be described by a 3×3×3 matrix. 27 components of the 3D matrix can be reduced to 10 components due to the Kleinman symmetry [27]. The components of β_{total} are defined as the coefficients in the Taylor series expansion of the energy in the external electric field. When the external electric field is weak and homogeneous, this expansion becomes

$$E = E^0 - \mu_\alpha F_\alpha - 1/2\alpha_{\alpha\beta}F_\alpha F_\beta - 1/6\beta_{\alpha\beta\gamma}F_\alpha F_\beta F_\gamma + \ldots .$$

where E^0 is the energy of the unperturbed molecule, F_α is the field at the origin, μ_α, $\alpha_{\alpha\beta}$, and $\beta_{\alpha\beta\gamma}$ are the components of the dipole moment, polarizability, and first order hyperpolarizability respectively. Using *x*, *y*, *z* components, the total static dipole moment μ, the mean dipole polarizability ⟨α⟩, the anisotropy of the polarizability Δα, and the total first order hyperpolarizability β_{total} are defined as

$$\mu = (\mu_x^2 + \mu_y^2 + \mu_z^2)^{1/2}, \qquad \langle\alpha\rangle = \frac{\alpha_{xx} + \alpha_{yy} + \alpha_{zz}}{3},$$

$$\Delta\alpha = 2^{-1/2}[(\alpha_{xx} - \alpha_{yy})^2 + (\alpha_{yy} - \alpha_{zz})^2 + (\alpha_{zz} - \alpha_{xx})^2 + 6\alpha_{xx}^2]^{1/2},$$

$$\beta_{total} = (\beta_x^2 + \beta_y^2 + \beta_z^2)^{1/2} \text{ and}$$

$$\beta_x = \beta_{xxx} + \beta_{xyy} + \beta_{xzz}, \qquad \beta_y = \beta_{yyy} + \beta_{xxy} + \beta_{yzz}, \qquad \beta_z = \beta_{zzz} + \beta_{xxz} + \beta_{yyz}.$$

The HF, DFT/B3LYP results of the electronic dipole moment μ_i ($i = x, y, z$), the polarizability α_{ij}, and the first order hyperpolarizability β_{ijk} are listed in Table 3. The calculated dipole moment of heptachlor is approximately found as 2.2 D for the methods used. Heptachlor does not have a large dipole moment because it has a relatively homogeneous charge distribution with the contribution of a lone pair located on Cl atoms. The highest value of the dipole moment is observed for the μ_y component. The DFT/B3LYP calculated anisotropy of the polarizability Δα of heptachlor is 5.4062×10^{-23} esu. However, the mean polarizability of heptachlor is found to be 2.8657×10^{-23} esu. This value is predicted to be 1.0946 times larger than that calculated by the HF method. The hyperpolarizability magni-

Table 3

Calculated μ, α, *and* β *components for heptachlor*

Parameters	B3LYP	HF	Parameters	B3LYP	HF
β_{xxx}	87.4289	44.4113	μ_x	0.1954	0.3148
β_{xxy}	–19.5737	0.4022	μ_y	1.9553	1.9122
β_{xyy}	28.9639	17.0463	μ_z	–0.8878	–1.1178
β_{yyy}	–69.4229	–20.3172	μ (Debye)	2.1563	2.2372
β_{xxz}	–19.1084	–12.2752	α_{xx}	210.092	192.522
β_{xyz}	–6.4911	–5.0583	α_{xy}	–9.096	–8.958
β_{yyz}	–29.6003	–14.6458	α_{yy}	188.032	170.352
β_{xzz}	–6.7548	1.0323	α_{xz}	11.233	11.635
β_{yzz}	–20.6798	–3.3975	α_{yz}	–2.267	–3.142
β_{zzz}	–88.3133	–56.8366	α_{zz}	181.969	167.095
β_{total} (esu)	1.7878×10^{-30}	0.9250×10^{-30}	$\langle\alpha\rangle$ (esu)	2.8657×10^{-23}	2.6180×10^{-23}
			Δα (esu)	5.4062×10^{-23}	4.9546×10^{-23}

N o t e. (α and β values of the Gaussian 03W output are reported in atomic units (a.u.) and converted to electrostatic units (esu). 1 a.u. = 0.1482×10^{-24} esu (for α); 1 a.u. = = 8.6393×10^{-33} esu (for β)).

tude is one of the key factors in a non-linear optical (NLO) system. The mean dipole polarizability $\langle\alpha\rangle$ gives also information about the electron distribution in a molecule. The DFT/B3LYP calculated first order hyperpolarizability value β_{total} of heptachlor is 1.7878×10^{-30} esu. HF calculated β_{total} is 1.9327 times smaller than that given by B3LYP. Large values of the polarizability and hyperpolarizability components indicate a substantial delocalization of charges in the given directions. As can be seen from Table 3, the HF method produces smaller values for the calculated parameters than DFT/B3LYP.

Atomic charge and electron density distributions of heptachlor in the gas and solution phases. Atomic charges computed by the Mulliken method [28, 29] and the electron density of heptachlor at the DFT/B3LYP and TD-DFT/B3LYP levels of theory in vacuum and ethanol are listed in Table 4. The magnitudes of the carbon atomic charges for heptachlor in vacuum and ethanol were found to be both positive and negative at the basis set. C(2), C(7), and C(8), which are acceptor atoms, exhibit a substantial positive charge whereas C(1), C(3), C(4), C(5), C(9), C(10), and C(11), which are donor atoms, exhibit a substantial negative charge. DFT/B3LYP calculations in ethanol result in that the atomic charges of C(1), C(2), C(5), C(7), C(8), C(9), C(10), and C(11) atoms increase whereas the atomic charges of C(3) and C(4) atoms decrease, as compared to the results obtained in vacuum. However, the TD-DFT/B3LYP method shows that the atomic charges of C(5), C(7) and C(11) increase due to the inductive effect of the solvent whereas the others decrease, as compared to the results obtained by the DFT/B3LYP method in ethanol.

The positive values of hydrogen atomic charges in both vacuum and ethanol indicate the charge transfer from hydrogen atoms to the others. The solvent effect seems to increase the atomic charges of the hydrogen atoms.

Atomic charges of chlorine atoms show discrepancies, depending on which atoms are connected to which atoms. As can be seen from Table 4, Cl(6), Cl(12), and Cl(13) atoms, which behave as donors, are negatively charged whereas Cl(15), Cl(14), Cl(17), and Cl(16) atoms, which behave as acceptors, are positively charged. The mesomeric effect as a result of π orbitals around C(9)=C(10) makes Cl(16) and Cl(17) atoms be positively charged and C(9) and C(10) atoms be negatively charged. A similar result can be seen for C(1), C(5), H(18), and H(19) atoms. It is clear from the differences in the atomic charges of chlorine atoms that steric hindrance caused by the non-planar geometry and electrostatic interactions play an important role in determining the atomic charges of heptachlor. The DFT/B3LYP calculation shows that Cl(6) and Cl(12) gain charge whereas the other chlorine atoms lose their charges in ethanol. However, the TD-DFT/B3LYP method produces an increase

Table 4

Mulliken atomic charges and electron density of heptachlor in vacuum and ethanol calculated by DFT/B3LYP *and* TD-DFT/B3LYP *methods with the* 6-311++G(*d*,*p*) *basis set*

Atoms	DFT/B3LYP (in vacuum)		DFT/B3LYP (in ethanol)		TD-DFT/B3LYP (in ethanol)	
	Atomic charge	Electron density	Atomic charge	Electron density	Atomic charge	Electron density
C(1)	–1.055	24.097	–1.057	24.048	–1.038	24.036
C(2)	0.687	38.502	0.690	38.832	0.658	38.795
C(3)	–0.794	19.326	–0.759	19.206	–0.743	19.352
C(4)	–0.711	26.886	–0.668	27.097	–0.661	26.975
C(5)	–0.282	26.198	–0.321	26.123	–0.336	26.176
Cl(6)	–0.010	17.504	–0.067	17.605	–0.055	17.615
C(7)	1.384	64.505	1.406	63.198	1.407	62.845
C(8)	1.641	57.996	1.671	57.396	1.653	57.439
C(9)	–1.297	21.293	–1.301	20.897	–1.278	20.965
C(10)	–0.874	17.901	–0.883	17.596	–0.873	17.539
C(11)	–0.405	74.522	–0.430	75.098	–0.447	75.018
Cl(12)	–0.202	20.445	–0.203	20.545	–0.202	20.609
Cl(13)	–0.278	19.233	–0.277	19.265	–0.281	19.276
Cl(14)	0.107	20.604	0.062	20.472	0.074	20.482
Cl(15)	0.242	20.957	0.206	20.699	0.214	20.709
Cl(16)	0.395	19.409	0.382	19.320	0.375	19.352
Cl(17)	0.339	20.695	0.334	20.552	0.322	20.663
H(18)	0.183	0.511	0.208	0.480	0.209	0.481
H(19)	0.246	0.649	0.265	0.625	0.262	0.631
H(20)	0.248	0.568	0.261	0.556	0.261	0.557
H(21)	0.252	0.569	0.275	0.544	0.274	0.545
H(22)	0.183	0.511	0.207	0.484	0.206	0.485

in the charge of negatively charged chlorine atoms and a decrease in the charge of positively charged chlorine atoms.

As can be seen from Table 4, the electron densities of chlorine atoms are almost equal (≈20). The Cl(6) atom has a comparatively less electron density due to the presence of the H(19) atom linked to C(2). As a result of the substitution of chlorine atoms, the electron densities of C(2), C(7), C(8), and C(11) atoms are relatively larger. The π bond between C(9) and C(10) does not allow these atoms to have an excess electron density even if they are linked to chlorine atoms.

HOMO and LUMO analysis. The HOMO characterizes the ability of electron giving; LUMO characterizes the ability of electron accepting. In addition, the HOMO energy is directly related to the ionization potential, while the LUMO energy is directly related to the electron affinity. The LUMO—HOMO energy gap gives information about the kinetic stability, chemical reactivity, optical polarizability, and chemical hardness-softness of a molecule [30, 31]. In order to evaluate the energy behavior of heptachlor, the HOMO and LUMO energies were calculated by TD-DFT/B3LYP, B3LYP, HF, LDA, and GGA methods and can be seen in Table 5 and Fig. 2. The 3D HOMO and LUMO graphs of

Table 5

Calculated orbital energy values of heptachlor in vacuum and the solvent phase

Parameter	B3LYP [a]	LDA [a]	GGA [a]	B3LYP (in ethanol)	TD-DFT/B3LYP (in chloroform)	TD-DFT/B3LYP (in ethanol)	TD-DFT/B3LYP (in water)
E_{HOMO}, eV	–7.5237	–5.8874	–5.7602	–7.4484	–7.4543	–7.4418	–7.4399
E_{LUMO}, eV	–1.6621	–1.8588	–1.6893	–1.6207	–1.6071	–1.6030	–1.6028
$\Delta E_{LUMO\text{-}HOMO}$	5.8616	4.0285	4.0710	5.8277	5.8472	5.8388	5.8371
Dipole moment, D	2.1563	1.4708	1.5478	3.0036	2.6975	2.9441	2.9940

[a] Calculated in the vacuum phase.

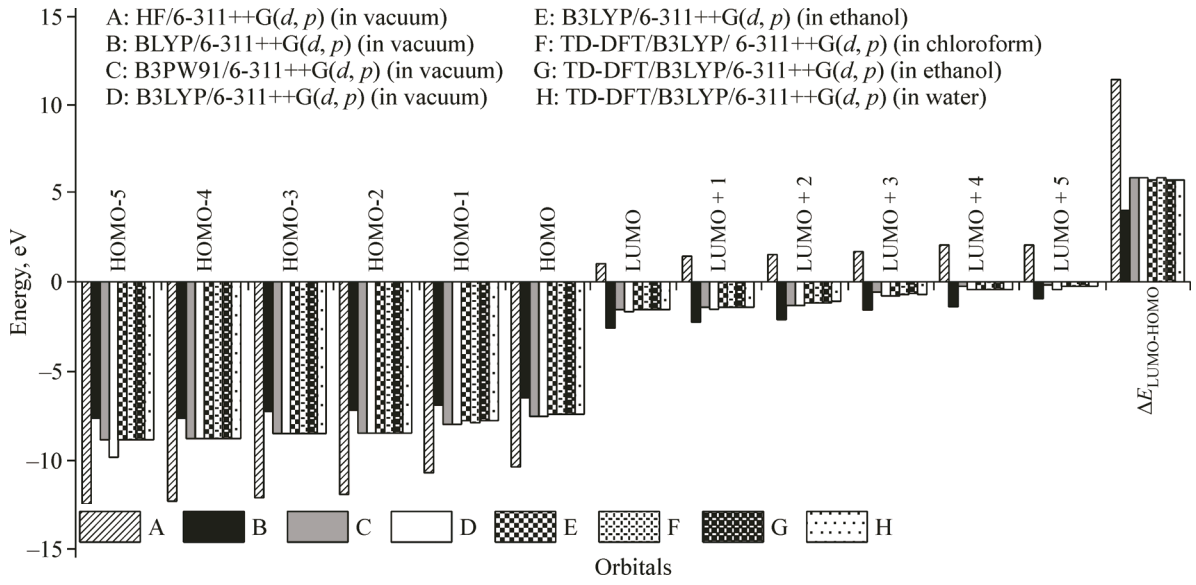

Fig. 2. Selected HOMO and LUMO energies calculated at different methods in vacuum and various solvents

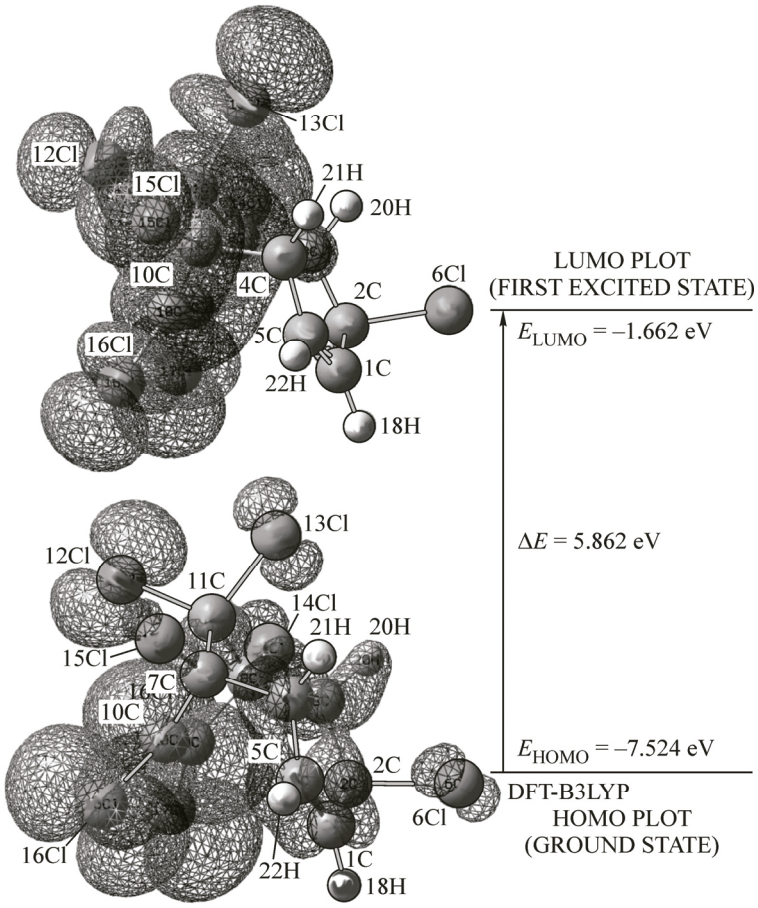

Fig. 3. 3D plots of HOMO and LUMO calculated by B3LYP/6-311++G(*d*,*p*) (in vacuum) for heptachlor

heptachlor calculated at the DFT/B3LYP level of theory are shown in Fig. 3. The positive phase is red and the negative phase is green. Both HOMOs and LUMOs are mostly σ-type orbitals. DFT and TD-

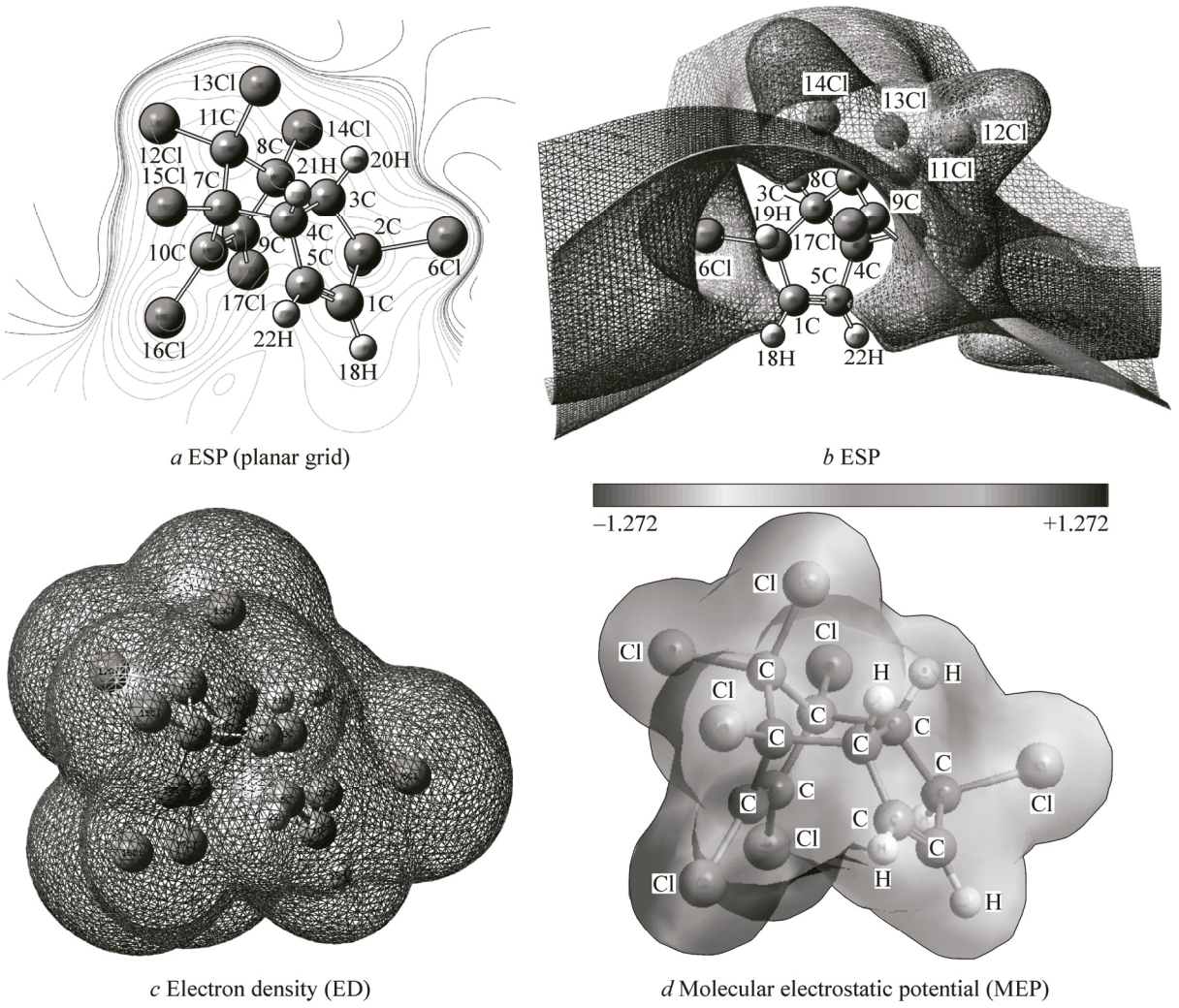

Fig. 4. 3D plots of (*a*) electrostatic potential (ESP in planar grid), (*b*) electrostatic potential (ESP) map, (*c*) electron density (ED) and (*d*) molecular electrostatic potential (MEP) map of heptachlor

DFT calculations in vacuum and the solvent phase predict $\Delta E \approx 5.8$ eV. These values indicate that heptachlor is kinetically unstable and biologically active. Furthermore, on passing from the gas phase to the solvent phase, the decreasing value of the energy gap indicates that haptachlor becomes unstable. As can be seen from Fig. 3, the HOMO is localized over the entire molecule. As can be seen from the LUMO plot, the C(1)—C(2)—C(3)—C(4)—C(5) ring and the Cl(6) atom give electrons to C(1)=C(5) and C(9)=C(10) bonds along with the other Cl atoms. The presence of Cl atoms makes heptachlor more reactive with its environment.

Electrostatic potential, total electron density, molecular electrostatic potential, and solvent accessible surface of heptachlor. In the present study, the electrostatic potential (ESP), total electron density (ED), molecular electrostatic potential (MEP), and solvent accessible surface of heptachlor calculated at the DFT/B3LYP-6-311++G(*d*,*p*) level of theory are illustrated in Figs. 4 and 5 respectively.

The ED plot shows a uniform distribution (Fig. 4, *c*). As can be seen from the ESP figure (Fig. 4, *a* and *b*), negative ESP is localized over the molecule and is reflected as a yellowish blob. ESP is a measure of the electronegativity and partial charges of the molecule.

MEP is a plot of the electrostatic potential drawn based on the constant electron density surface and is a very useful descriptor in determining sites for the electrophilic attack and nucleophilic reactions as well as hydrogen bonding interactions [32, 33]. The importance of MEP lies in the fact that

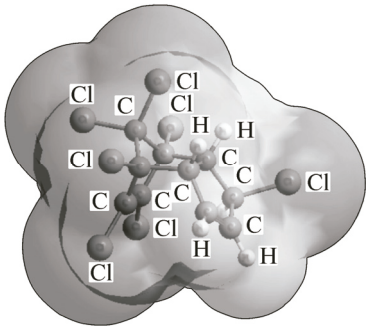

Fig. 5. Solvent accessible surface of heptachlor

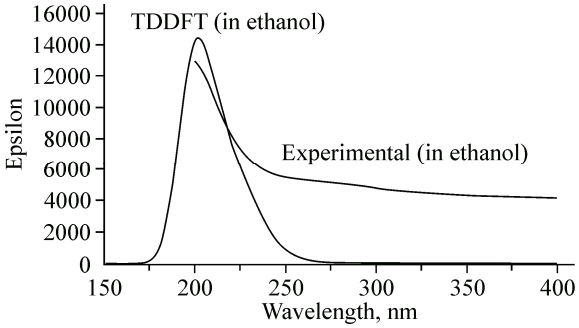

Fig. 6. Experimental and TD-DFT/B3LYP-6-311++G(*d*,*p*) calculated UV-vis. spectra of heptachlor

it simultaneously displays the molecular size and shape as well as positive, negative, and neutral electrostatic regions in terms of color grading (Fig. 4, *d*) and is very useful research tool for the molecular structure with its physicochemical property relationship [38—42]. Different ESP values on the surface are represented by different colors. The negative MEP regions were related to the electrophilic reactivity and the positive regions were related to the nucleophilic reactivity (Fig. 4, *d*). As can be seen from heptachlor MEP, the negative regions are mainly localized around chlorine atoms, except for Cl(6) that has only a positive potential. The regions having a positive potential are over the hydrogen atoms.

The solvent accessible surface of heptachlor is displayed in Fig. 5. The green regions show the interactions of chlorine atoms with the solvent, while the gray regions indicate the interactions of hydrogen atoms with the solvent. The magnitude of green regions is larger than that of the gray ones. It is clear from Fig. 5 that the interaction between heptachlor and the solvent is mostly controlled by chlorine atoms.

Electronic absorption spectra. All molecules allow strong σ—σ* and π—π* transitions in the UV-vis region with high extinction coefficients. The chemical structure of heptachlor is composed of single bonds along with two double bonds. Based on a fully optimized ground-state structure, TD-DFT/B3LYP/6-311++G(*d*,*p*) calculations have been used to determine the low-lying excited states of heptachlor in water, ethanol, chloroform, and cyclohexane solvents. The solvent effect was calculated by means of IEFPCM, which is the SCRF method [34, 35]. Experimental and theoretically obtained UV-vis spectra of heptachlor in ethanol are depicted in Fig. 6. It could be seen that the absorption band of heptachlor in ethanol is observed at 201 nm (Fig. 6). The visible absorption maxima of the compound correspond to the electron transition between HOMO and LUMO. At the TD-DFT/B3LYP/6-311++G(*d*,*p*) level of theory λ_{max} were observed in the range of 203 nm. The peaks calculated in this

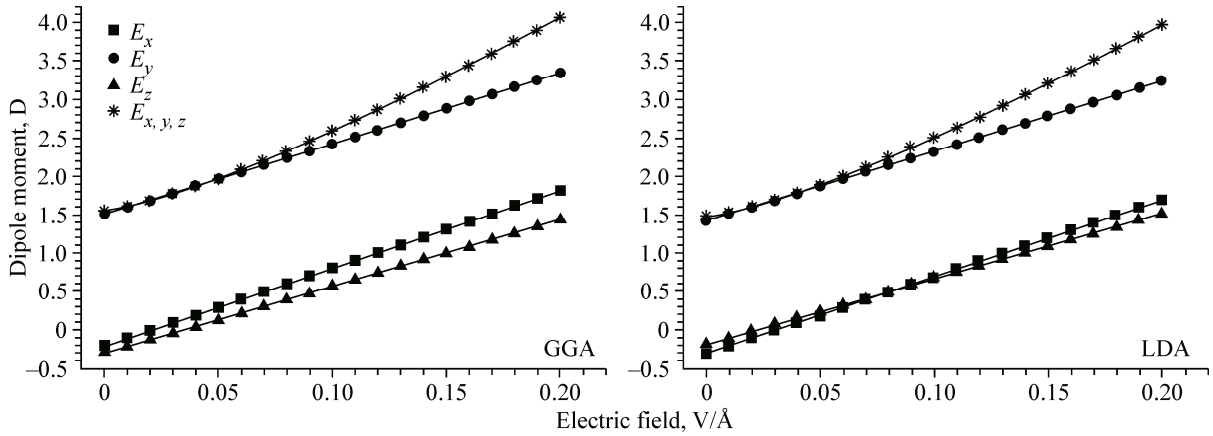

Fig. 7. Dipole moment versus applied external electric field (EF) calculated by using GGA and LDA methods

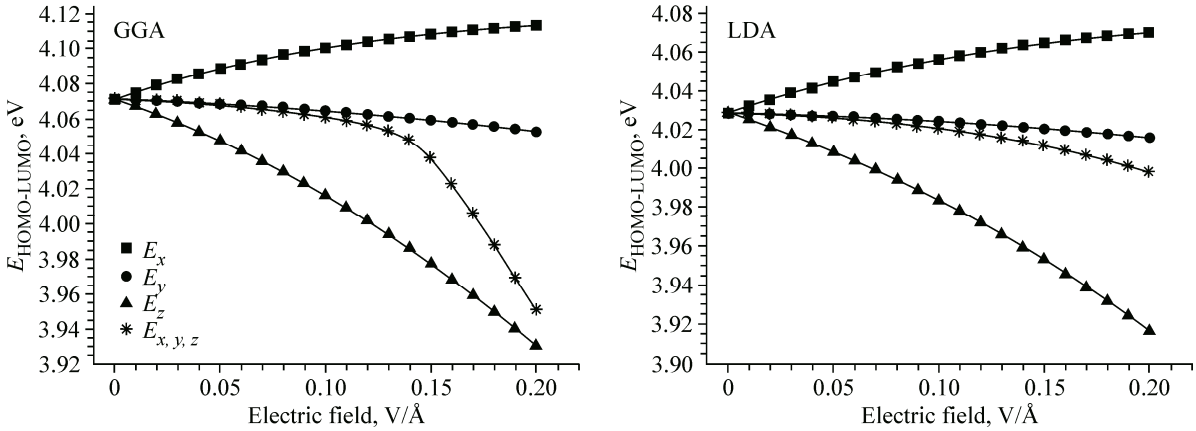

Fig. 8. $E_{\text{HOMO-LUMO}}$ gap versus applied external electric field (EF) calculated by using GGA and LDA methods

range are attributed to dipole-allowed σ—σ* type transitions. This result was also supported by the analysis of the orbital population (Fig. 3).

Electric field effect on E_{HOMO}—E_{LUMO} (ΔE) and dipole moment (Debye). Figs. 7 and 8 show a change in the dipole moment and the HOMO-LUMO gap (ΔE) with the applied external electric field on a heptachlor molecule. According to Fig. 7, the force of the applied electric field increases as the dipole moment of the heptachlor molecule increases. We can say that the density and orientation of the molecular charge change with alteration and direction of the electric field. Moreover, all electrons in the heptachlor molecule are withdrawn to electronegative atoms. Thus, the molecular bonding increases its polarity. The electric field applied to the molecule brings about a pronounced charge transfer. The toxic properties of this molecule increase.

As seen in Fig. 8, the fundamental HOMO-LUMO gap value is 4.071 eV according to the GGA calculation. If the difference between the LUMO and HOMO energies decreases due to the increasing force of the electric field, the charge transfer in the molecule comes into existence very easily. The LUMO level is dominant with the C character along with some contribution coming from the Cl character. As seen in Fig. 3, the contribution coming from the H character is very small. A similar relationship corresponds to the HOMO level.

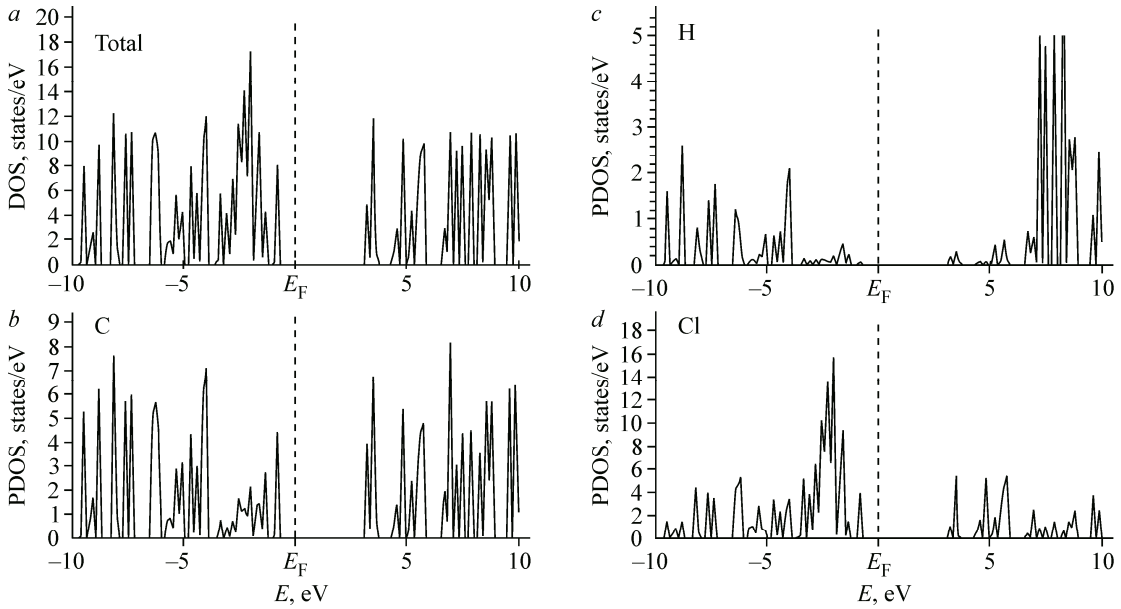

Fig. 9. Density of states (DOS) of heptachlor. Vertical dotted lines indicate the Fermi level E_F

Density of states. Electron densities of states (DOS) and partial densities of states (PDOS) for the heptachlor molecule reported here are given in Fig. 9. The energy is given with respect to the Fermi level E_F, indicated by dashed lines in Fig. 9. Although we calculated the electronic structure with LDA and GGA, here only GGA results are given. Our GGA results say that the heptachlor molecule does not show spin polarization.

CONCLUSIONS

The UV-vis. spectra of heptachlor have been analyzed by the TD-DFT method in the solvent phase. Molecular orbital analysis suggests that the calculated absorption maximum value is predicted as the σ—σ* electronic transition. The NBO result reflects the charge transfer due to C—C and Cl—C groups. The nonlinear optical behavior of the titled molecule was investigated by the determination of the dipole moment μ, the mean polarizability ⟨α⟩, and the first order hyperpolarizability β_{total}. It is observed that heptachlor has the β_{total} and Δα values of about 10^{-30} esu. and 10^{-23} esu. respectively. MEP shows that the negative potential sites are mainly located on chlorine atoms while the regions having the positive potential are over the hydrogen atoms. The solvent accessible surface indicates that the interaction of heptachlor with the solvent is mostly controlled by chlorine atoms. The electron density analysis in vacuum and the solvent phase indicates that carbon atoms linked to chlorine atoms have a relatively higher electron density.

The authors thank the Bitlis Eren University, Scientific and Technological Application and Research Center for supporting the research facilities.

REFERENCES

1. US Public Health Service, US Department of Health and Human Services, Agency for Toxic Substances and Disease Registry (ATSDR), Toxicological profile for chlordane (Draft), Atlanta, GA, 1992.
2. US Public Health Service, US Department of Health and Human Services, Agency for Toxic Substances and Disease Registry (ATSDR), Toxicological profile for heptachlor: heptachlor epoxide, Atlanta, GA, 1993.
3. US Public Health Service, US Department of Health and Human Services, Agency for Toxic Substances and Disease Registry (ATSDR), Toxicological profile for toxaphene, Atlanta, GA, 1990.
4. Concise International Chemical Assessment Document; 70. Heptachlor. First draft prepared by Drs. J. Keilhorn, S. Schmidt and I. Mangelsdorf, Fraunhofer Institute of Toxycology and Experimental Medicine, Hanover, Germany; and Dr. P. Howe, Centre of Ecology and Hydrology, Monks Wood, United Kingdom; World Health Organization, Switzerland, 2006.
5. *Steffneyi E.R., Peter M.Y., Linda F.C. et al.* // Toxic. Let. – 1999. – **104**. – P. 127 – 135.
6. *Kerkhoff M., de Boer J., Geerdes J.* // Sci. Total Environ. – 1981. – **19**. – P. 41 – 50.
7. *Becker P.R., Mackey E.A., Demiralp R. et al.* // Chemosphere. – 1997. – **34**. – P. 2067 – 2098.
8. *Stehr-Green P.A., Wohlleb J.C., Royce W. et al.* // J. Am. Med. Assoc. – 1988. – **259**, N 3. – P. 374 – 377.
9. *Salman M.D., Reif J.S., Rupp L. et al.* // J. Toxicol. Environ. Health. – 1990. – **31**, N 2. – P. 125 – 132.
10. *Mora M.A.* // Arch. Environ. Toxicol. – 1996. – **31**. – P. 533 – 537.
11. International Programme on Chemical Safety (IPSC), Persistent organic pollutants assessment report. Inter Organization Programme for the Sound Management of Chemicals (IOMC), 1995.
12. *Reuber M.D.* // J. Toxicol. Environ. Health. – 1979. – **5**, N 4. – P. 729 – 748.
13. *Reuber M.D.* // J. Environ. Pathol. Toxicol. Oncol. – 1987. – **7**, N 3. – P. 85 – 114.
14. US Environmental Protection Agency, Integrated Risk Information System (IRIS) on Chlordane, Environmental Criteria and Assessment Office, Office of Health and Environmental Assessment, Office of Research and Development, Cincinnati, OH, 1993.
15. *Telang S., Tong C., Williams G.M.* // Carcinogenesis. – 1982. – **3**. – P. 1175 – 1178.
16. *Ruch R.J., Fransson R., Flodstrom S. et al.* // Carcinogenesis. – 1990. – **11**, N 7. – P. 1097 – 1101.
17. *Kang K.S., Wilson M.R., Hayashi T. et al.* // Environ. Health Perspect. – 1996. – **104**, N 2. – P. 192 – 200.
18. *Soler J.M., Artacho E., Gale J.D. et al.* // J. Phys.: Condens. Matter. – 2002. – **14**. – P. 2745 – 2779.
19. *Perdew J.P., Zunger A.* // Phys. Rev. B. – 1981. – **23**. – P. 5048 – 5079.
20. *Zhang Y., Yang W.* // Phys. Rev. Lett. – 1998. – **80**. – P. 890.
21. *Perdew L.P., Burke K., Ernzerhof M.* // Phys. Rev. Lett. – 1996. – **77**. – P. 3865 – 3868.
22. *Troullier N., Martins J.L., Troullier N. et al.* // Phys. Rev. B. – 1991. – **43**. – P. 1993 – 2006.

23. *Kleinman L., Bylander D.M.* // Phys. Rev. Lett. – 1982. – **48**. – P. 1425 – 1428.
24. *Frisch M.J. et al.* // Gaussian 09, Revision A.1, Gaussian, Inc., Wallingford CT, 2009.
25. *Shields K.G., Kennard C.H.L.* // J. Chem. Soc., Perkin Trans. – 1973. – **2**. – P. 1374 – 1376.
26. *Durig J.R., Little T.S., Gounev T.K. et al.* // J. Mol. Struct. – 1996. – **375**. – P. 83 – 94.
27. *Huyskens F.L., Huyskens P.L., Person A.P.* // J. Chem. Phys. – 1998. – **108**. – P. 8161 – 8171.
28. *Olsen J., Jørgensen P.J.* // J. Chem. Phys. – 1985. – **82**. – P. 3235 – 3264.
29. *Helgaker T.U., Jensen H.J.A., Jørgensen P.J.* // J. Chem. Phys. – 1986. – **84**. – P. 6280 – 6284.
30. *Gülseven Sıdır Y., Sıdır İ.* // J. Mol Struct. – 2013. – 1**045**. – P. 131 – 138.
31. *Gülseven Sıdır Y., Sıdır İ., Taşal E. et al.* // Int. J. Quant. Chem. – 2011. – **111**. – P. 3616 – 3629.
32. *Scrocco E., Tomasi J.* // Adv. Quantum Chem. – 1978. – **11**. – P. 115 – 193.
33. *Luque F.J., Lopez J.M., Orozco M.* // Theor. Chem. Acc. – 2000. – **103**. – P. 343 – 345.
34. *Wong M.W., Frisch M.J., Wiberg K.B.* // J. Am. Chem. Soc. – 1991. – **113**. – P. 4776 – 4782.
35. *Cances E., Mennucci B., Tomasi J.* // J. Chem. Phys. – 1997. – **107**, N 8. – P. 3032 – 3041.